# Dynamics of tachyon dark energy on large scales and its imprint on the observed galaxy power spectrum

Ajay Bassi,[1,*] Ankan Mukherjee,[2,1,†] and Anjan A. Sen[3,1,‡]

[1]*Centre for Theoretical Physics, Jamia Millia Islamia, New Delhi 110025, India*
[2]*Department of Physics, Bangabasi College, Kolkata 700009, India*
[3]*School of Arts and Sciences, Ahmedabad University, Ahmedabad 380009, India*

(Received 17 April 2021; accepted 17 May 2021; published 9 June 2021)

In the present work, we study the large scale matter power spectrum as well as the observed galaxy power spectrum for a noncanonical tachyon field dark energy model considering the full general relativistic perturbation equations. We form a set of coupled autonomous equations, including both the background and linearly perturbed quantities, and obtain their solutions numerically with proper set of initial conditions. We consider different scalar field potentials for our study. Deviations from the concordance Λ cold dark matter (ΛCDM) model are studied for different relevant quantities. Our study shows that the noncanonical tachyon dark energy model produces enhanced gravitational potentials and comoving density contrast, as well as linear growth factor for matter perturbations compared to ΛCDM. It is also observed that, for tachyon dark energy models, there is suppression of power on large scales compared to both the ΛCDM model as well as previously studied canonical scalar field models.

DOI: 10.1103/PhysRevD.103.123522

## I. INTRODUCTION

The observed phenomenon of late time cosmic acceleration [1,2] has brought a drastic change in our understanding of the present universe. The genesis of cosmic acceleration is not yet firmly established. An exotic component dubbed as "dark energy" can be introduced in the energy budget of the Universe to produce the desired repulsive gravitational effect. In addition to the dark energy cosmology, modified gravity theories are also introduced to explain the cosmic acceleration (for comprehensive review, see [3]).

Among different theoretical prescriptions to explain late time cosmic acceleration, the dark energy cosmology is found to be the most consistent with astronomical observations. However, we hardly have the knowledge about the actual physical entity of dark energy. Cosmological constant or vacuum energy density are potential candidates of dark energy [4–6]. The cosmological constant (Λ) along with cold dark matter (CDM) is known as the concordance ΛCDM model. Though the ΛCDM model is consistent with most of the cosmological observations [7], there are certain theoretical issues, like the fine-tuning problem, as well as the cosmic coincidence problem. Apart from this, some of the recent astronomical observations, mainly the local measurement of Hubble constant ($H_0$) [8] and the direct measurements of the fluctuations in the matter density distribution in the Universe ($S_8$) by Kilo-Degree Survey + VISTA Kilo-Degree Infrared Galaxy Survey spanning 450 degree$^2$ + Dark Energy Survey Y1 [9], are in tension with the Planck-ΛCDM estimation of those parameters. For all these reasons, time-evolving dark energy models are also well emphasized in the literature. In the case of time-evolving dark energy, the potential candidates are different canonical and noncanonical scalar fields [10–13] or some exotic fluid with specific equation of state [14]. For a comprehensive review of different time-evolving dark energy models, we refer the reader to [15].

In the present work, we study the evolution of cosmological perturbations in a tachyon dark energy model. Tachyon is a noncanonical description scalar field dark energy. A tachyon scalar field was invoked in the context of dark energy by Padmanabhan [13]. Many more discussions on tachyon dark energy are there in literature [16–21]. Spherical collapse of matter overdensity in tachyon dark energy is studied by Rajvanshi and Bagla [22] and by Setare *et al.* [23]. Effects of inhomogeneous tachyon dark energy on cosmological perturbations are studied by Singh *et al.* [24].

It is an important task in dark energy cosmology to distinguish the time-varying dark energy model from the cosmological constant. A possible way to accomplish this is to study the background expansion, as well as the evolution of cosmological perturbations. Cosmological perturbations in the matter field and its evolution can be studied from the temperature and polarization spectrum of the cosmic microwave background (CMB) [7] and also

*ajay@ctp-jamia.res.in
†ankan.ju@gmail.com
‡anjan.sen@ahduni.edu.in; aasen@jmi.ac.in

 

from the observed galaxy power spectrum [25]. CMB observation by Planck along with other observational data have ensured unprecedented constraints on cosmological parameters [7]. However, most of these observations probe subhorizon scale physics where the Newtonian approximations for cosmological perturbation is valid and the dark energy perturbations can be safely ignored. Thus, all the dark energy parameters, constrained in Planck observations, are related to the background evolution of dark energy. Future observations like the Large Synoptic Survey Telescope (LSST) [26], Square Kilometer Array (SKA) [27] will provide a wide redshift range sky survey in optical and radio observations and a much more sophisticated map of the distribution of matter in the Universe. These types of observations will be highly effective to study the general relativistic (GR) effects in the evolution of cosmological perturbations, where the inhomogeneities in dark energy could not be ignored. As the cosmological constant ($\Lambda$) is homogeneous, these future observations would be the smoking gun to distinguish the cosmological constant from the time-varying dark energy models and would also be effective to check the viability of various dark energy models.

As already mentioned, the present analysis is carried out for tachyon dark energy. The full general relativistic effects on the evolution of linear perturbations and galaxy power spectrum are studied. We formulate a set of autonomous system of equations, which are studied numerically with proper initial conditions. Quintessence scalar field dark energy perturbation and its scale dependence was studied by Unnikrishnan *et al.* [28]. In case of tracker quintessence, the galaxy power spectrum incorporating GR corrections and its imprint on the neutral hydrogen distribution in the Universe are studied by Duniya *et al.* [29]. Dinda and Sen have studied the galaxy power spectrum in inhomogeneous thawing scalar field dark energy [30]. Recently, Singh *et al.* [24] have studied the perturbations in tachyon dark energy and its effects on the clustering of dark matter, and a comparative study of linear perturbation in quintessence and tachyon is carried out by Rajvanshi *et al.* [31].

The paper is organized as follows. In Sec. II, the background evolution equations for the present models are discussed. The perturbation equations with general relativistic corrections and their solutions are discussed in Sec. III. In Sec. IV, the different power spectrums and their deviation from $\Lambda$CDM at different redshift are presented. Finally, in Sec. V, we conclude with an overall discussion about the results.

## II. BACKGROUND EVOLUTION

A noncanonical description of scalar field dark energy, namely the tachyon, is studied in the present work. We consider Dirac-Born-Infeld–type action to study the dynamics of the tachyon scalar field

$$\mathcal{S} = \int -V(\phi)\sqrt{1-\partial^{\mu}\phi\partial_{\mu}\phi}\sqrt{-g}d^4x. \tag{1}$$

Here $V(\phi)$ is the potential for noncanonical scalar field $\phi$. The energy density and pressure of the tachyon scalar field are, respectively, given by [17]

$$\bar{\rho}_{\phi} = \frac{V(\phi)}{\sqrt{1-\dot{\phi}^2}}, \tag{2}$$

$$\bar{P}_{\phi} = -V(\phi)\sqrt{1-\dot{\phi}^2}, \tag{3}$$

where the overhead dot represents the derivative with respect to cosmic time. From the action, given in Eq. (1), the equation of motion for scalar field is obtained as

$$\ddot{\phi} + 3H\dot{\phi}(1-\dot{\phi}^2) + \frac{V_{,\phi}}{V}(1-\dot{\phi}^2) = 0, \tag{4}$$

where subscript "$,\phi$" is the derivative with respect to the scalar field $\phi$. The Hubble parameter ($H$) in a spatially flat Friedmann-Lemaître-Robertson-Walker (FLRW) universe is expressed as

$$H^2 = \frac{\bar{\rho}_{\phi} + \bar{\rho}_m}{3}, \tag{5}$$

where $\bar{\rho}_m$ is the energy density of the background matter, which includes the contribution from both the dark matter and baryons.

## III. RELATIVISTIC PERTURBATION

We consider a conformal Newtonian gauge with vanishing anisotropic stress for the flat FLRW spacetime with perturbed metric

$$ds^2 = a^2(\tau)[(1+2\Phi)d\tau^2 - (1-2\Phi)d\vec{x}.d\vec{x}], \tag{6}$$

where $\tau$ is the conformal time, $a(\tau)$ is the conformal scale factor, $\vec{x}$ are the comoving coordinates, and $\Phi$ is the gravitational potential. The linearized Einstein equations obtained for the above perturbed metric [Eq. (6)] are written as [30]

$$\nabla^2\Phi - 3\mathcal{H}(\Phi' + \mathcal{H}\Phi) = 4\pi G a^2 \sum_i \delta\rho_i, \tag{7}$$

$$\Phi' + \mathcal{H}\Phi = 4\pi G a^2 \sum_i (\bar{\rho}_i + \bar{P}_i)v_i, \tag{8}$$

$$\Phi'' + 3\mathcal{H}\Phi' + (2\mathcal{H}' + \mathcal{H}^2)\Phi = 4\pi G a^2 \sum_i \delta P_i, \tag{9}$$

where prime denotes the derivative with respect to the conformal time $\tau$, $\bar{P}_i$ and $\bar{\rho}_i$ represent the background

pressure and energy density of each component, namely the matter and tachyon filed, and $\mathcal{H}$ denotes the conformal Hubble parameter. $\delta P_i$, $\delta\rho_i$, and $v_i$ are the linear order perturbed quantities for the background pressure, energy density, and velocity field, respectively. $\vec{v_i} = -\vec{\nabla} v_i$ defines the irrotational component of the velocity field. From Eqs. (7) and (8), one gets the relativistic Poisson equation as

$$\nabla^2\Phi = 4\pi G a^2 \sum_i \bar{\rho_i}\,\Delta_i, \tag{10}$$

where $\Delta_i = \delta_i + 3\mathcal{H}(1+w_i)v_i$ represents the gauge-invariant comoving energy density contrast for the $i$th component. $\Delta_i$ is the correct tracer for the gravitational potential on large scales. The relativistic continuity and Euler equations can be obtained from the conservation of stress-energy tensor as [30]

$$\delta' + 3\mathcal{H}\left(\frac{\delta P}{\delta\rho} - \frac{\bar{P}}{\bar{\rho}}\right)\delta = \left(1+\frac{\bar{P}}{\bar{\rho}}\right)(\theta + 3\Phi'), \tag{11}$$

and

$$\theta' + 3\mathcal{H}\left(\frac{1}{3} - \frac{\bar{P}'}{\bar{\rho}'}\right)\theta = \frac{\nabla^2\delta P}{\bar{\rho}+\bar{P}} + \nabla^2\Phi, \tag{12}$$

respectively, where $\theta = -\vec{\nabla}.\vec{v}$ and $\delta = \frac{\delta\rho}{\bar{\rho}}$. Finally the evolution equations of perturbed energy density, pressure, and velocity at linear order for tachyon scalar field are given as

$$\delta\rho_\phi = \frac{V(\phi)}{(1-\dot{\phi}^2)^{3/2}}(\dot{\phi}\dot{\delta\phi} - \Phi\dot{\phi}^2) + \frac{V_\phi\delta\phi}{\sqrt{1-\dot{\phi}^2}}, \tag{13}$$

$$\delta P_\phi = \frac{V(\phi)}{\sqrt{1-\dot{\phi}^2}}(\dot{\phi}\dot{\delta\phi} - \Phi\dot{\phi}^2) - V_\phi\delta\phi\sqrt{1-\dot{\phi}^2}, \tag{14}$$

$$a(\bar{\rho_\phi} + \bar{P_\phi})v_\phi = V(\phi)\frac{\dot{\phi}\delta\phi}{\sqrt{1-\dot{\phi}^2}}. \tag{15}$$

Next, we define the following dimensionless parameters related to the background and perturbed quantities for the tachyon field:

$$\begin{aligned}
&x = \dot{\phi}, \qquad y = \frac{\sqrt{V(\phi)}}{\sqrt{3}H},\\
&\lambda = -\frac{V_{,\phi}}{V^{3/2}}, \qquad \Gamma = V\frac{V_{,\phi\phi}}{(V_{,\phi})^2},\\
&\delta\phi = \frac{\dot{\phi}}{H}q, \qquad \Omega_\phi = \frac{y^2}{\sqrt{1-x^2}},\\
&\gamma_\phi = 1+\omega_\phi = \dot{\phi}^2 = x^2.
\end{aligned} \tag{16}$$

The $x$ here is just a dimensionless parameter and is different from the comoving coordinates in Eq. (6). $\Omega_\phi$ is the density parameter and $w_\phi$ is the equation of state parameter for the tachyon scalar field $\phi$. We can now form a set of autonomous system of equations involving the quantities defined in Eq. (16) to study the different quantities associated with both the background and perturbed universe [32],

$$\begin{aligned}
\gamma_\phi' &= -6\gamma_\phi(1-\gamma_\phi) + 2\sqrt{3\gamma_\phi\Omega_\phi}\lambda(1-\gamma_\phi)^{5/4},\\
\Omega_\phi' &= 3\Omega_\phi(1-\gamma_\phi)(1-\Omega_\phi),\\
\lambda' &= -\sqrt{3\gamma_\phi\Omega_\phi}\lambda^2(1-\gamma_\phi)^{1/4}(\Gamma - 3/2),\\
\mathcal{H}' &= -\frac{1}{2}(1+3\Omega_\phi(\gamma_\phi - 1))\mathcal{H},\\
\Phi' &= \Phi_1,\\
q' &= q_1,\\
\Phi_1{}' &= -(1+B)\Phi_1 - \left(2B - 3 + \frac{3}{2}\Omega_\phi\gamma_\phi\right)\Phi\\
&\quad + \frac{3}{2}\Omega_\phi\gamma_\phi[q_1 + q(3\gamma_\phi - B + g(1-\gamma_\phi))],\\
q_1{}' &= -(g - 3\gamma_\phi - B)q_1 - B_q q - (3\gamma_\phi - 4)\Phi_1\\
&\quad + (g - 6\gamma_\phi)\Phi.
\end{aligned} \tag{17}$$

Here prime represents derivative with respect to $N = log(a)$. We have defined $B = 1.5(1-(\gamma_\phi - 1)\Omega_\phi)$, $g = 2\lambda\sqrt{\frac{3\Omega_\phi}{\gamma_\phi}}(1-\gamma_\phi)^{1/4}$, and $B_q = -B' + (g - 6\gamma_\phi)(3-B) + \frac{k^2}{\mathcal{H}^2}(1-\gamma_\phi)$.

Matter density contrast and peculiar velocity for matter are obtained from the Fourier space solutions of Eqs. (7), (8), (13), and (15) as

$$\begin{aligned}
\delta_m &= -\frac{2}{\Omega_m}\left[\Phi_1 + \Phi\left(1 - \frac{\Omega_\phi\gamma_\phi}{2(1-\gamma_\phi)} + \frac{k^2}{3\mathcal{H}^2}\right)\right.\\
&\quad \left. + \frac{\Omega_\phi\gamma_\phi}{2(1-\gamma_\phi)}(q_1 + q(3\gamma_\phi - B)\right],\\
y_m &= 3\mathcal{H}v_m = \frac{2}{\Omega_m}[\Phi_1 + \Phi - 1.5q\Omega_\phi\gamma_\phi].
\end{aligned} \tag{18}$$

Using Eq. (18), we can define the gauge-invariant comoving matter density contrast as $\Delta_m = \delta_m + y_m$.

### A. Initial conditions

One needs to set the initial conditions for $(\gamma, \Omega_\phi, \lambda, \mathcal{H})$ for the background universe and $(\Phi, \Phi', q, q')$ for the perturbed universe to solve the set of autonomous equations defined in Eqs. (17). We fix the initial conditions at decoupling epoch ($z = 1000$), when the universe was matter dominated and contribution from dark energy was negligible. For this, we follow the same procedure as described in [30]. The scalar field is frozen initially at $w_\phi \sim -1$ due to large Hubble friction [$3H\dot{\phi}$ term in Eq. (4)], such that $\gamma_i \sim 0$, but we set it at very small value $\gamma_i = 10^{-7}$. $\Omega_\phi$ is negligible initially at $z = 1000$ because the universe was matter dominated. $\lambda$ gives the slope of the potential and determines the evolution of the scalar field. We set $\lambda_{\rm in} \ll 1$ so that the scalar field remains frozen to the initial value of equation of state $\omega_\phi \sim -1$ and behaves like a cosmological constant initially. We fix the initial values of $\Omega_\phi, \lambda$, and $\mathcal{H}$ in a manner so that we get the desired values of $\Omega_{\phi 0}$ and $\mathcal{H}_0$ at present redshift $z = 0$.

One can ignore the contribution of dark energy at $z = 1000$ as the universe was matter dominated at that redshift, and hence we set $q = \frac{dq}{dN} = 0$ initially. Moreover, the gravitational potential $\Phi$ being constant during matter domination, we set the initial value of gravitational potential using Eq. (10) and relation $\Delta_m \sim a$ (during matter domination) as

$$\Phi_{\rm in} = -\frac{3}{2}\frac{\mathcal{H}_{\rm in}^2}{k^2} a_{\rm in}, \tag{19}$$

which is a constant, and hence $\frac{d\Phi}{dN} = 0$ initially.

### B. Behavior of cosmological parameters

To get the desired results, we fix $\Omega_{m0} = 0.28, \lambda_i = 0.7$, and $\mathcal{H}_0 = 70$ km/s/Mpc. These values are consistent with different cosmological observations including CMB by Planck, and the overall behavior of our final results are not sensitive to these values. With the initial conditions set as above, we solve the set of autonomous Eqs. (17) and study the dynamics of the different cosmological parameters. We are considering power-law potentials, more specifically, linear, inverse, and inverse-squared potentials.

In Fig. 1, we show the behavior of equation of state parameter $(\omega_\phi = \gamma_\phi - 1)$ as a function of redshift for the different potentials. We set the identical initial conditions for all the potentials and $\phi$ remains frozen at $\omega_\phi = -1$ initially and thaws away from cosmological constant-type behavior in the near past.

In Fig. 2, we study the behavior of gravitational potential in comparison to the ΛCDM case. We show the percentage deviation in the gravitational potential $\Phi$ of the tachyon

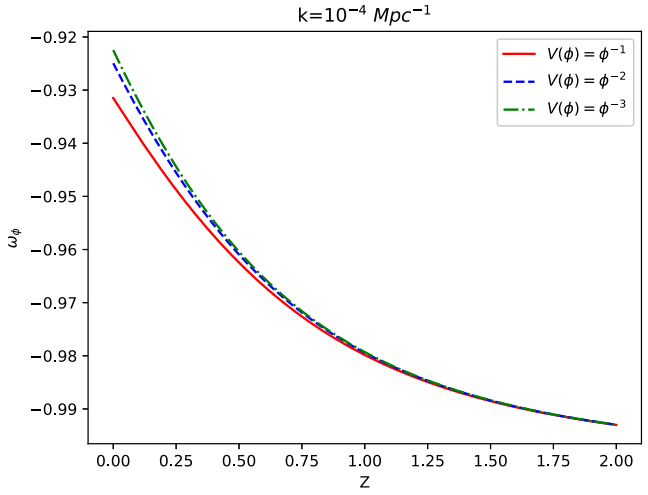


FIG. 1. Equation of state for the tachyon scalar field $w_\phi$ as a function of redshift $z$ at large scale $k = 10^{-4}$ Mpc$^{-1}$ and for different potentials with $\Omega_{m0} = 0.28$ and $\lambda_i = 0.7$.

dark energy from the ΛCDM model for different types of potentials. For redshifts $z \neq 0$, the deviation is less than 1% for all scales, whereas for $z = 0$, the deviation is around 3%–4% for large scales and around 1% at small scales. Also the linear potential results in the highest deviation compared to other potentials. This is similar to the canonical scalar dark energy model [30]. We should stress that the small scale behavior in the tachyon dark energy model is primarily governed by its background evolution, whereas on the large scales, effect of perturbation in tachyon field plays a significant role.

In Fig. 3, we study the behavior of the gauge-invariant matter density contrast $\Delta_m$. The behavior is similar to the gravitational potential, but with comparatively smaller deviation from the ΛCDM case.

Next, we define the quantity $f$ which depends on the velocity field perturbations and gives rise to the redshift space distortion

$$f = -\frac{k^2 v_m}{\mathcal{H}\Delta_m}. \tag{20}$$

In Fig. 4, we show the deviatin in $f$ from ΛCDM model for different scalar field potentials. For redshift $z = 0$, the deviation in $f$ is smaller than 6%, and for higher redshifts, the deviation is even smaller for all potentials considered. There is hardly any scale dependency, which shows that the contribution to the deviation in $f$ is from background expansion only.

## IV. THE OBSERVED GALAXY POWER SPECTRUM

Considering the different aspects of galaxy distribution, we can study the evolution of our Universe. Newtonian perturbations are enough to study the underlying dark

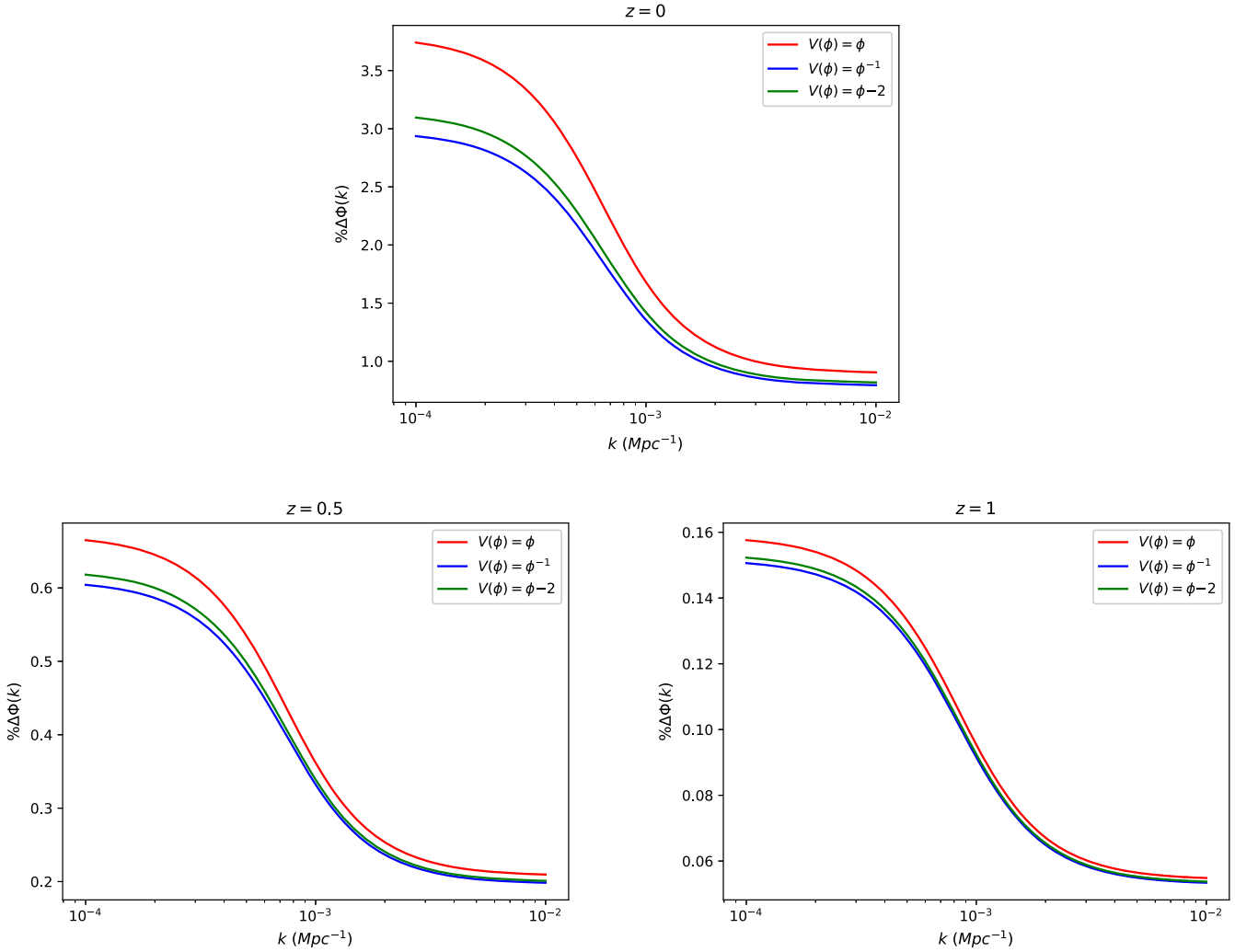


FIG. 2. Percentage deviation in gravitational potential $\Phi$ from $\Lambda$CDM model as a function of $k$ with $\Omega_{m0} = 0.28$ and $\lambda_i = 0.7$. Here and in subsequent plots, we use $\%\Delta X = (X^{\phi}/X^{\Lambda} - 1) \times 100$.

matter distribution on subhorizon scales. On horizon scales, we need full general relativistic treatment to study the effects of dark energy perturbations on dark matter distribution. It will help us to distinguish between different dark energy models from modified gravity models.

We see the galaxies in the redshift space and the galaxy distribution is influenced by the peculiar velocities of the galaxies in addition to the dark matter fluctuations. This gives rise to Kaiser redshift space distortion [33], which is a measure of large scale velocity fields. The gravitational potential in the metric [Eq. (6)] can affect the photon geodesics by integration along the path and gives rise to the gravitational lensing effect. This effect alters the galaxy distribution and results in magnification bias [34].

In the recent past, people have shown that the general relativistic treatment on large scales can affect the observed galaxy distribution by contributing to how the gravitational potential, velocity fields, and matter density affect the observed number density of galaxies on large scales [35–40]. These general relativistic effects are negligible on small subhorizon scales but are significant on large scales and help to distinguish between different dark energy models from modified gravity models.

All the above effects play important parts in the observed fluctuations in the number of galaxies across the sky at different redshifts and angles. The galaxy number overdensity $\Delta^o$ incorporating these effects can be written as [29,36,38,41]

$$\Delta^o = \left[b + f\mu^2 + \mathcal{A}\left(\frac{\mathcal{H}}{k}\right)^2 + i\mu\mathcal{B}\left(\frac{\mathcal{H}}{k}\right)\right]\Delta_m, \quad (21)$$

where $b$ is the bias parameter on linear scales, $f$ is the redshift space distortion parameter, $\mu = \frac{\vec{n}\cdot\vec{k}}{k}$ with $\vec{n}$ gives the direction of observation, and $\vec{k}$ is the wave vector with magnitude $k$. The parameters $\mathcal{A}$ and $\mathcal{B}$, which arise due to full general relativistic treatment, are given by

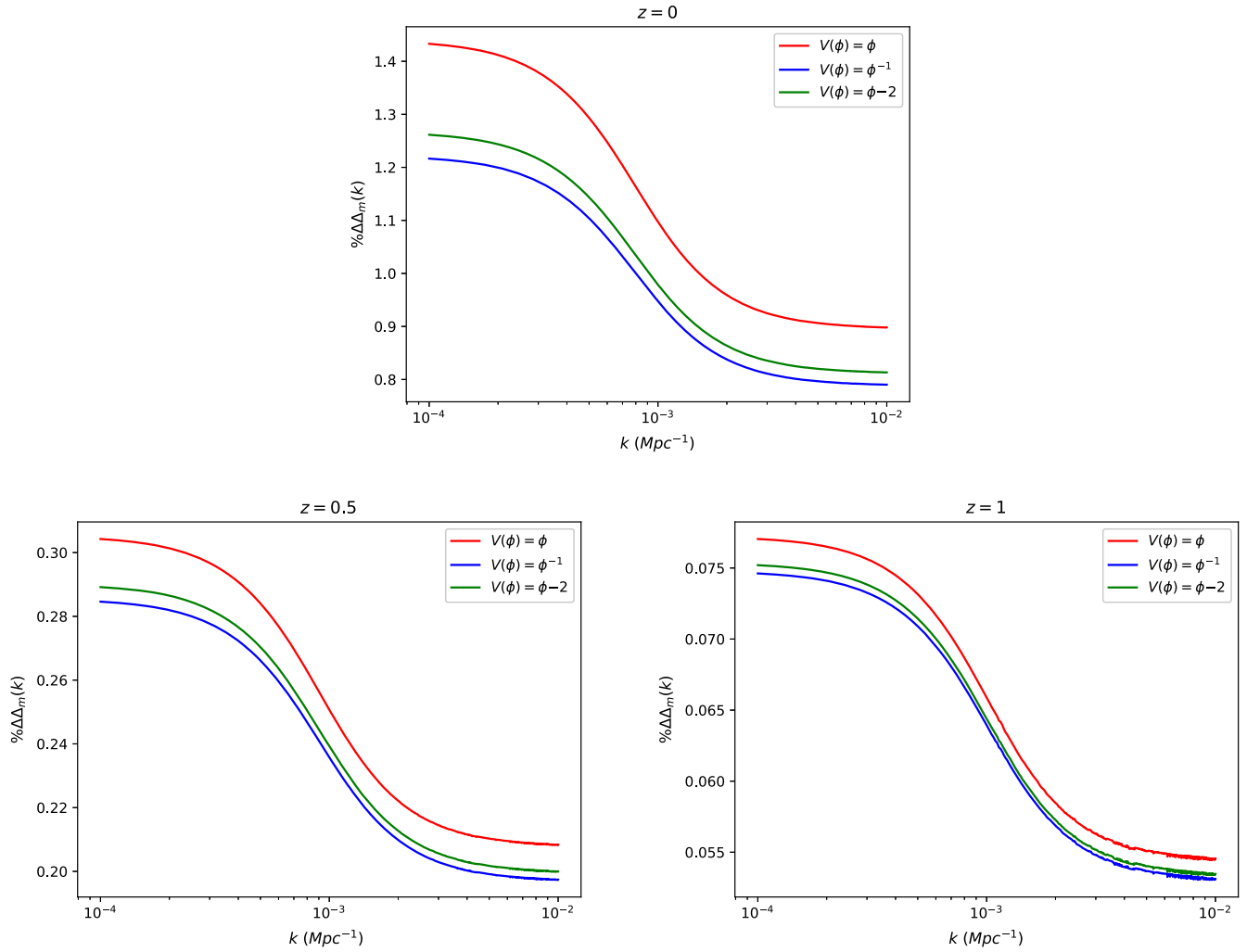


FIG. 3. Percentage deviation in comoving density contrast $\Delta_m$ from ΛCDM model as a function of $k$.

$$\mathcal{A} = 3f + \left(\frac{k}{\mathcal{H}}\right)^2 \left[3 + \frac{\mathcal{H}'}{\mathcal{H}^2} + \frac{\Phi'}{\mathcal{H}\Phi}\right] \frac{\Phi}{\Delta_m}, \tag{22}$$

$$\mathcal{B} = -\left[2 + \frac{\mathcal{H}'}{\mathcal{H}^2}\right] f. \tag{23}$$

We have assumed constant comoving galaxy number density, thus galaxy evolution bias is zero in our case and we have considered magnification bias $b = 1$ [41]. We have neglected time delay, integrated Sachs-Wolfe effect, and weak lensing integrated terms in our calculations. In Eq. (21), the first term inside the square bracket is related to the galaxy bias, the second term is the Kaiser redshift term, and the third and fourth terms are purely due to the general relativistic corrections. In the last two terms, $\mathcal{A}$ [given by Eq. (22)] is related to the peculiar velocity fields [Eq. (20)] and gravitational potential, and $\mathcal{B}$ is related to the Doppler effect.

We can write the power spectrum for the observed galaxy number overdensity using Eq. (21) (only real part) as [29,35]

$$P(k,z) = P_s(k,z)\left[(b + f\mu^2)^2 + 2(b + f\mu^2)\left(\frac{\mathcal{A}}{x^2}\right) + \frac{\mathcal{A}^2}{x^4} + \mu^2\left(\frac{\mathcal{B}^2}{x^2}\right)\right], \tag{24}$$

where $x = \frac{k}{\mathcal{H}}$ and $P_s(k,z)$ is the standard matter power spectrum,

$$P_s(k,z) = Ak^{n_s - 4}T(k)^2\left(\frac{|\Delta_m(k,z)|}{|\Phi(k,0)|}\right)^2. \tag{25}$$

We can also define the power spectrum with only the Kaiser redshift space distortion term included as

$$P_{ks}(k,z) = (b + f\mu^2)^2 P_s(k,z). \tag{26}$$

In the standard matter power spectrum given by Eq. (25), $A$ is fixed by $\sigma_8$ normalization. We use the Eisenstein-Hu

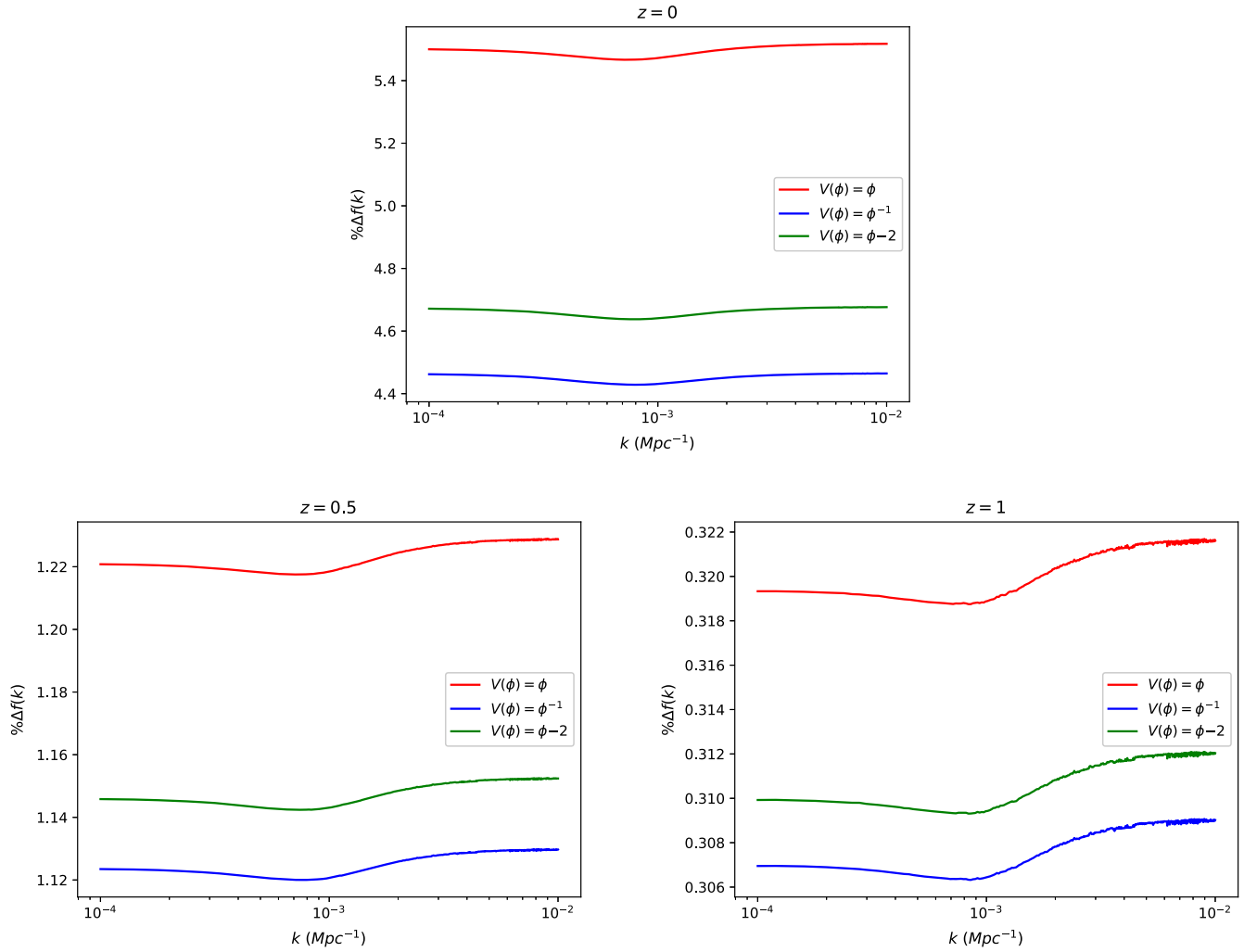


FIG. 4. Percentage deviation in $f$ from ΛCDM model as a function of $k$.

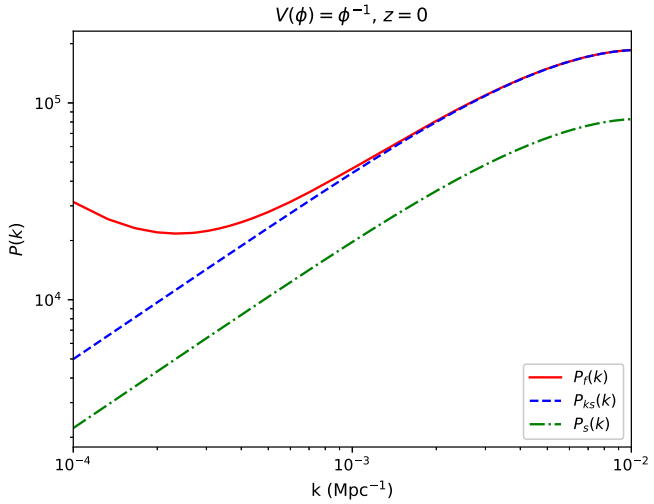


FIG. 5. Continuous, dashed, and dash-dotted lines for the full observed galaxy power spectrum $P(k)$ given by Eq. (24), the galaxy power spectrum $P_{ks}(k)$ by taking only the Kaiser redshift term [first term inside the square bracket in Eq. (24)], and the standard matter power spectrum $P_s(k)$ given by Eq. (25) as a function of $k$.

transfer function $T(k)$ [42] in our case. In Fig. 5, we have plotted the line of sight ($\mu = 1$) for the observed galaxy power spectrum at $z = 0$ for linear potentials only by using Eq. (24). We put the spectral index for the initial power spectrum $n_s = 0.98, \sigma_8 = 0.8, \Omega_{bo} = 0.05, \Omega_{mo} = 0.28$, and $h = 0.7$ using $\sigma_8$ normalization.

In Fig. 5, we have plotted the observed galaxy power spectrum with and without general relativistic corrections. When the Kaiser redshift space distortion term is considered, the power spectrum $P_{ks}(k, z)$ shifts with an almost constant factor to higher values on all scales compared to the standard matter power spectrum. When general relativistic corrections are considered, then the total power spectrum remains almost equal with $P_{ks}(k, z)$ on small scales, but shows substantial enhancement to higher values on large scales, which again shows that the GR corrections contribute on large scales.

In Fig. 6, we have shown the percentage deviation in the standard matter power spectrum $P_s(k, z)$, the power spectrum with only the Kaiser term $P_{ks}(k, z)$, and the total power spectrum $P(k, z)$ from the ΛCDM model on

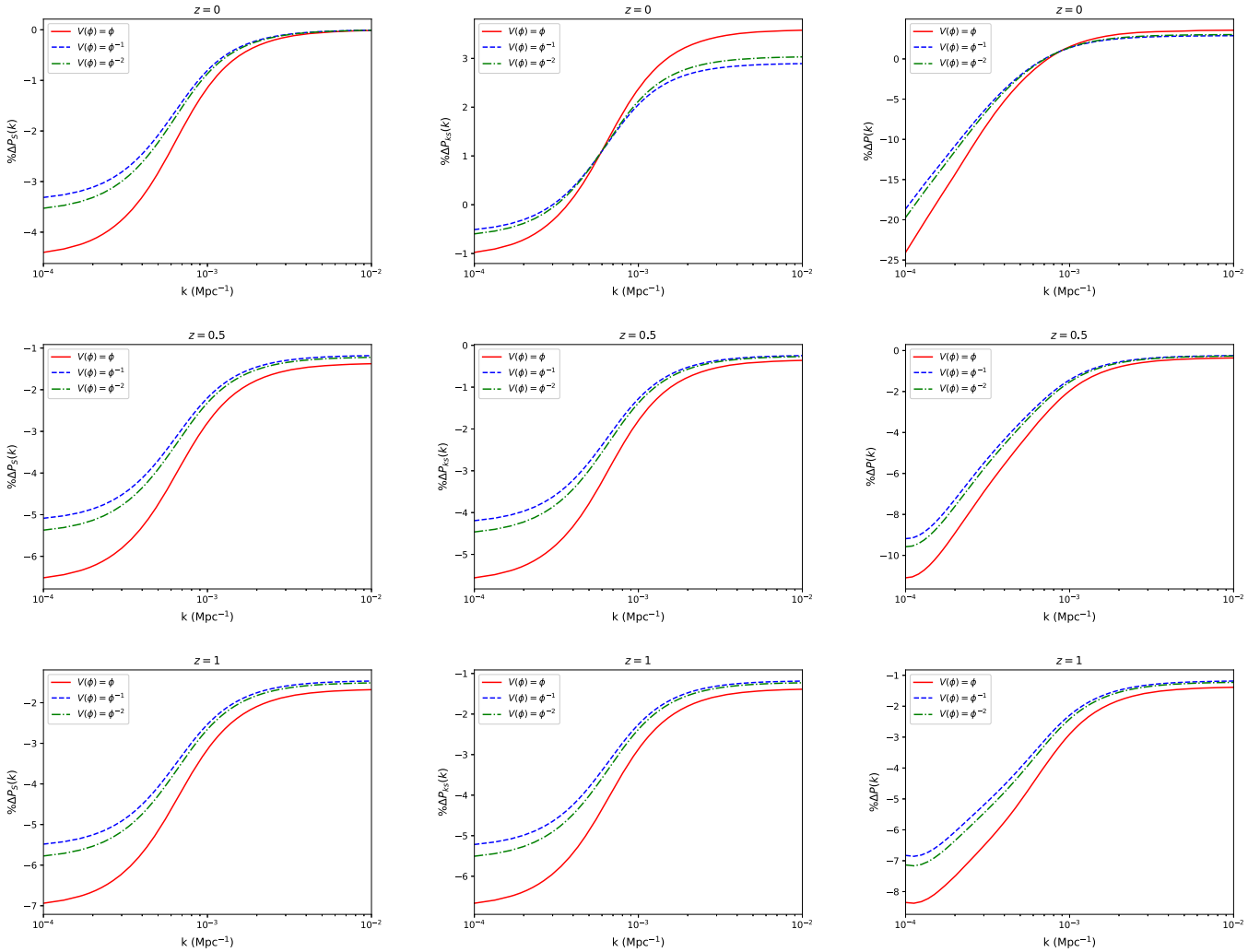


FIG. 6. Percentage deviation in power spectrum $P(k)$ from ΛCDM model for different scalar field potentials and for different redshifts as a function of $k$. The left column is for the deviation in standard matter power spectrum $P_s(k)$ given by Eq. (25), the middle column is for the deviation in the power spectrum with the Kaiser redshift space distortion term $P_{ks}(k)$, and the right column is for the full observed galaxy power spectrum $P(k)$ given by Eq. (24).

different scales $k$ for different redshifts and for different scalar field potentials.

From Eq. (25), we can observe how $P_s(k,z)$ depends upon $\Delta_m$ and $\Phi$. From Fig. 3, except at $z=0$ where there is slight enhancement in $\Delta_m$ in the tachyon model compared to ΛCDM, for other redshifts, the deviation in $\Delta_m$ from ΛCDM is negligible. On the other hand, the gravitational potential $\Phi$ has a reasonable enhancement in the tachyon model compared to ΛCDM at $z=0$ on large scales. With this, from Eq. (25), one expects the suppressions in $P_s(k,z)$ in the tachyon model compared to ΛCDM on large scales, which is shown in the left column in Fig. 6.

Next we consider the power spectrum with the Kaiser redshift space distortion term $P_{ks}(k,z)$ [Eq. (26)]. It depends upon the growth function $f$ given by Eq. (20). In Fig. 4, we have shown that there is an enhancement in $f$ in the tachyon model compared to ΛCDM for large redshift and this enhancement is largely scale dependent. For smaller redshifts, the enhancement is minimal. This reflects the effect in $P_{ks}(k,z)$ [Eq. (26)], as shown in the middle column in Fig. 6.

Finally, we consider the full power spectrum $P(k,z)$ with general relativistic corrections given by Eqs. (22) and (23). The deviation in $P(k,z)$ from the ΛCDM model is large on large scales due to the contribution of dark energy perturbations on large scales and small redshifts through the $\Phi$ term (the scalar field model starts behaving like matter-only model for higher redshifts). For redshift $z=0$, at large scale, the suppression from ΛCDM is around 17%–24% depending upon different scalar field potentials. However, if we look at at the smaller scale at $z=0$, we observe a slightly higher $P(k)$ for the present model than the corresponding ΛCDM. At nonzero redshift, the $P(k)$ remains suppressed even at smaller scale. Comparing this

to the deviation in $P_{ks}(k,z)$, we can see that the GR corrections highly suppress the power spectrum at larger scale. At smaller scale, the deviation in $P(k,z)$ has similar behavior as in $P_{ks}(k,z)$ due to the negligible contribution of the GR corrections on small scales. The effect of GR corrections is maximum around present day. We should also stress that, for the full power spectrum $P(k,z)$ with general relativistic corrections, deviation from ΛCDM in the tachyon model is much larger than the corresponding deviations in canonical scalar field models [30] as well as cubic Galilean models [43]. This is why tachyon models can be more easily distinguished from ΛCDM compared to canonical scalar field as well as Galilean models.

It worth mentioning at this point that some earlier works have also emphasized the perturbation in tachyon dark energy and their effects on cosmic large scale structures. Singh *et al.* [24] have discussed the perturbations in tachyon dark energy and their effects on the clustering of matter. They have studied the evolution of gravitational potential, density contrast of dark matter, and dark energy for inverse-squared and exponential potential. In the present work, we have adopted linear, inverse, and inverse-squared potential. In [24], it was observed that the effect of dark energy perturbations is significant only at superhorizon scale and it causes the enhancement of gravitational potential and the growth of density contrast at superhorizon scale for tachyon dark energy compared to that of ΛCDM. These results are totally consistent with the findings of the present work. Additionally, in the present work, we have also emphasized the nature of matter power spectrum for tachyon dark energy considering the fully relativistic perturbation equations. Substantial suppression of power is observed at large scale in the case of tachyon dark energy. In another recent article, Rajvanshi *et al.* [31] have compared the linear perturbations in tachyon and quintessence dark energy and their impacts on the observational measurements of cosmological parameters from cosmic microwave background. It was found that these two models, namely the tachyon and quintessence, are not distinguishable at background and linear perturbation level. In the present work, we have shown that the fully relativistic analysis of the matter and dark energy perturbations enable us to distinguish the present model from ΛCDM. The study of matter power spectrum using the nonlinear equations of tachyon dark energy perturbations is one of the new aspects of the present study. Similar analysis for thawing quintessence dark energy has been carried by Dinda and Sen [30]. A close observation of the results from the present analysis and the results in [30] would reveal that, though the suppression of power spectrum in the case of tachyon and quintessence from the ΛCDM have similar patterns, the amount of suppressions of power spectrum is not the same in tachyon and quintessence. Thus, the comparison of fully relativistic matter power spectrum could successfully break the degeneracy of quintessence and tachyon dark energy cosmology.

## V. CONCLUSION

The present work deals with the relativistic perturbations in a tachyon field dark energy model. The prime emphasis is on the nature of cosmological perturbations considering the full general relativistic corrections. The GR corrections are important at large scales where the inhomogeneity in dark energy distribution is no longer negligible. We have formed a set of coupled dynamical equations involving the relevant quantities of background and perturbed universe. The solutions of the set of dynamical equations are studied with proper initial conditions.

The gravitational potential ($\Phi$) is found to be slightly higher than that of ΛCDM (Fig. 2). The deviation is higher at large scales, where GR corrections effectively contribute. The deviation is higher at $z = 0$. The comoving matter density contrast also shows a similar profile of deviation from the ΛCDM (Fig. 3). The linear growth rate of matter perturbation ($f$) is also found to be higher for the present model than the ΛCDM and the deviation is maximum at $z = 0$ (Fig. 4). Further, we have studied power spectrum of matter density contrast and observed galaxy power spectrum for the present model and also investigated the difference in the power spectrum from the ΛCDM power spectrum (Figs. 5 and 6). Suppression in power in the matter power spectrum $[P_s(k)]$ compared to the ΛCDM is observed and the power suppression is higher at large scale (left column of Fig. 6). The power is enhanced when the Kaiser redshift space distortion term is introduced in the power spectrum $[P_{ks}(k)]$ (middle column of Fig. 6). At large scales, $P_{ks}(k)$ remains suppressed compared to the ΛCDM model. However, at smaller scales and at $z = 0$, the $P_{ks}(k)$ for the present model overtakes the ΛCDM. At other redshifts, it is almost the same as compared to the ΛCDM curves at smaller scales. In the right column of Fig. 6, the deviation in the observed galaxy power spectrum from ΛCDM is shown. The observed galaxy spectrum is also suppressed in the present model at large scales. At smaller scales, it comes closer to the ΛCDM spectrum. It is apparent from the plots that the general relativistic corrections, which introduces the effect of dark energy inhomogeneity in cosmological perturbations, suppresses the matter power spectrum and observed galaxy power spectrum substantially at large scales. On the other hand, the power is not much affected by the GR corrections at smaller scales, as the dark energy inhomogeneity is not effective at those scales.

Future observations like SKA and LSST will observe the sky at much larger scale and at much higher redshift. For those observations, GR corrections in the cosmological perturbations are essential. At that scale of observation, the

inhomogeneity of dark energy distribution would have its signature on the matter field. Hence those observations will be highly effective to distinguish homogeneous dark energy (the ΛCDM) from time-varying dark energy, which allows the clustering of dark energy. Even different time-varying dark energy models could be distinguished in this method. Hence these type of studies are highly relevant in present cosmological research. Future observations in radio and optical regimes would be highly effective to reveal the nature of dark energy, as well as to give a better understanding about the physical entity of the dark energy.

## ACKNOWLEDGMENTS

A. B. acknowledges the financial support from the Council of Scientific and Industrial Research (CSIR), Government of India as a SRF (CSIR file No. 09/466 (0172)/2016-EMR-I). A. M. acknowledges the financial support from the Science and Engineering Research Board (SERB), Department of Science and Technology, Government of India as a National Postdoctoral Fellow (NPDF file No. PDF/2018/001859). A. A. S. acknowledges funding from DST-SERB, Government of India, under the project No. MTR/2019/000599.

[1] A. G. Riess *et al.* (Supernova Search Team), Astron. J. **116**, 1009 (1998).
[2] S. Perlmutter *et al.* (Supernova Cosmology Project Collaboration), Astrophys. J. **517**, 565 (1999).
[3] S. Tsujikawa, Lect. Notes Phys. **800**, 99 (2010).
[4] S. M. Carroll, Living Rev. Relativity **4**, 1 (2001).
[5] P. J. E. Peebles and B. Ratra, Rev. Mod. Phys. **75**, 559 (2003).
[6] T. Padmanabhan, Phys. Rep. **380**, 235 (2003).
[7] N. Aghanim *et al.* (Planck Collaboration), Astron. Astrophys. **641**, A6 (2020).
[8] A. G. Riess, S. Casertano, W. Yuan, L. M. Macri, and D. Scolnic, Astrophys. J. **876**, 85 (2019).
[9] M. Asgari, T. Tröster, C. Heymans, H. Hildebrandt, J. L. van den Busch, A. H. Wright, A. Choi, T. Erben, B. Joachimi, S. Joudaki *et al.*, Astron. Astrophys. **634**, A127 (2020).
[10] B. Ratra and P. J. E. Peebles, Phys. Rev. D **37**, 3406 (1988).
[11] S. Tsujikawa, Classical Quant. Grav. **30**, 214003 (2013).
[12] R. J. Scherrer, Phys. Rev. Lett. **93**, 011301 (2004).
[13] T. Padmanabhan, Phys. Rev. D **66**, 021301 (2002).
[14] M. C. Bento, O. Bertolami, and A. A. Sen, Gen. Relativ. Gravit. **35**, 2063 (2003).
[15] E. J. Copeland, M. Sami, and S. Tsujikawa, Int. J. Mod. Phys. D **15**, 1753 (2006).
[16] E. J. Copeland, M. R. Garousi, M. Sami, and S. Tsujikawa, Phys. Rev. D **71**, 043003 (2005).
[17] J. S. Bagla, H. K. Jassal, and T. Padmanabhan, Phys. Rev. D **67**, 063504 (2003).
[18] L. R. W. Abramo and F. Finelli, Phys. Lett. B **575**, 165 (2003).
[19] J. M. Aguirregabiria and R. Lazkoz, Phys. Rev. D **69**, 123502 (2004).
[20] Z. K. Guo and Y. Z. Zhang, J. Cosmol. Astropart. Phys. 08 (2004) 010.
[21] C. J. A. P. Martins and F. M. O. Moucherek, Phys. Rev. D **93**, 123524 (2016).
[22] M. P. Rajvanshi and J. Bagla, Classical Quant. Grav. **37**, 235008 (2020).
[23] M. R. Setare, F. Felegary, and F. Darabi, Phys. Lett. B **772**, 70 (2017).
[24] A. Singh, H. K. Jassal, and M. Sharma, J. Cosmol. Astropart. Phys. 05 (2020) 008.
[25] M. Tegmark *et al.* (SDSS Collaboration), Astrophys. J. **606**, 702 (2004).
[26] J. R. Foley *et al.* (LSST Collaboration), arXiv:1812.00514.
[27] R. Maartens *et al.* (SKA Cosmology SWG Collaboration), *Proc. Sci.*, AASKA14 (2015) 016 [arXiv:1501.04076].
[28] S. Unnikrishnan, H. K. Jassal, and T. R. Seshadri, Phys. Rev. D **78**, 123504 (2008).
[29] D. Duniya, D. Bertacca, and R. Maartens, J. Cosmol. Astropart. Phys. 10 (2013) 015.
[30] B. R. Dinda and A. A. Sen, Phys. Rev. D **97**, 083506 (2018).
[31] M. P. Rajvanshi, A. Singh, H. K. Jassal, and J. S. Bagla, arXiv:2104.00982.
[32] R. J. Scherrer and A. A. Sen, Phys. Rev. D **77**, 083515 (2008).
[33] N. Kaiser, Mon. Not. R. Astron. Soc. **227**, 1 (1987).
[34] R. Moessner, B. Jain, and J. V. Villumsen, Mon. Not. R. Astron. Soc. **294**, 291 (1998).
[35] D. Jeong, F. Schmidt, and C. M. Hirata, Phys. Rev. D **85**, 023504 (2012).
[36] A. Challinor and A. Lewis, Phys. Rev. D **84**, 043516 (2011).
[37] C. Bonvin, Classical Quant. Grav. **31**, 234002 (2014).
[38] D. Duniya, arXiv:1606.00712.
[39] D. Duniya, Gen. Relativ. Gravit. **48**, 52 (2016).
[40] J. Yoo, A. L. Fitzpatrick, and M. Zaldarriaga, Phys. Rev. D **80**, 083514 (2009).
[41] D. G. A. Duniya, D. Bertacca, and R. Maartens, Phys. Rev. D **91**, 063530 (2015).
[42] D. J. Eisenstein and W. Hu, Astrophys. J. **496**, 605 (1998).
[43] B. R. Dinda, W. Hossain, and A. A. Sen, J. Cosmol. Astropart. Phys. 01 (2018) 045.